

## REGIMES OF NON-PREMIXED FLAME-VORTEX INTERACTIONS

D. THÉVENIN,<sup>1</sup> P. H. RENARD,<sup>1</sup> G. J. FIECHTNER,<sup>2</sup> J. R. GORD<sup>3</sup> AND J. C. ROLON<sup>1</sup>

<sup>1</sup>*Laboratoire EM2C*

*Ecole Centrale Paris and CNRS*

*Grande Voie des Vignes*

*F-92295 Châtenay-Malabry, France*

<sup>2</sup>*Innovative Scientific Solutions, Inc.*

*2766 Indian Ripple Road*

*Dayton, OH 45440-3638, USA*

<sup>3</sup>*Propulsion Directorate*

*Air Force Research Laboratory*

*Wright-Patterson Air Force Base*

*OH 45433-7103, USA*

Detailed studies of flame-vortex interactions are extremely valuable to improve our understanding of turbulent combustion regimes. Combined experimental and numerical studies have already been performed in the premixed case during previous investigations. Therefore, we decided to carry out a detailed experimental investigation on the regimes observed during interaction of a vortex ring and a non-premixed, diluted, hydrogen/air, laminar counterflow flame. To obtain the needed information, several optical diagnostic techniques have been used, in particular, planar laser-induced fluorescence (PLIF) of acetone to quantify vortex structure and speed, simultaneous OH PLIF and Rayleigh measurements, and simultaneous OH PLIF and particle-imaging velocimetry (PIV) measurements. A post-processing of the results combined with direct simulations using detailed chemistry and transport models to check the quality of the postprocessing procedures has led to the construction of a spectral interaction diagram. Eight interaction types were found, emphasizing the relative importance of competing physical phenomena such as straining, curvature, wrinkling, roll-up, and extinction. In particular, we observe two different types of extinction, one due to the combined action of curvature and straining, and the other purely due to straining effects. It was also observed that many vortices are too small or dissipate too rapidly to influence the flame. In other cases, the vortex ring can lead to the formation of pockets of oxidizer burning in the fuel part of the domain. These regimes and the limits between them have important implications for the modeling of turbulent non-premixed combustion.

### Introduction

The interaction of flames and vortices is a problem of theoretical and practical interest. In particular, if a field of turbulence is considered to be a collection of vortices of different sizes and strengths, it is possible to use the flame-vortex interaction as a model problem to investigate basic processes associated with turbulent combustion. Flame-vortex interactions often govern the combustion rate or lead to combustion instabilities. Vortices are observed in free flames and in flames stabilized on bluff bodies or are used to enhance mixing.

Numerous publications can be found concerning flame-vortex interactions, and we refer to our previous papers on the subject [1–4]. Complementary information can be found, for example, in Refs. [5–10]. Considering these publications, one may conclude that the interaction of a premixed flame with a vortex ring or a counterrotating vortex pair has

been studied extensively. Efforts to identify different regimes and to compare experimental and numerical results in particular concerning the extinction limits have been successful [9,11,12].

Experiments using non-premixed flames are more difficult and initially were carried out in water using an acid-base reaction to simulate the flame [13] or employed quite different configurations such as jet flames submitted to natural or forced vortical instabilities [14–17]; more recently, burning rings [18,19] were studied under microgravity conditions. Considering that experiments on diffusion flames are in high demand, a counterflow burner was built in our laboratory to investigate the effect of vortices in non-premixed cases [1,20]. An international collaboration was initiated to obtain as many experimental measurements as possible for this configuration.

The present paper begins by providing details on the experimental setup. The postprocessing of the measurements is then described. Identified interaction regimes are subsequently shown and used to

construct an interaction diagram. Finally, the implications of these results for non-premixed turbulent combustion are discussed.

### Experimental Apparatus and Procedure

A detailed description of the counterflow burner was given in Ref. [20], and a schematic illustration of the setup may be found in Refs. [1] and [3]. Experiments were performed with hydrogen diluted with nitrogen on the upper side and air on the lower side, at room temperature and pressure. Each injection nozzle had a diameter of 25 mm and was surrounded by another nozzle issuing nitrogen to isolate the reactive stream from outer perturbations. A steady, non-premixed flame featuring a one-dimensional structure around the stagnation point was initiated. This flame was subjected to a constant low-level strain acting along its plane. The resulting strain rate was negligible compared to that exerted by the vortex rings.

We changed the global mixture ratio,  $\phi$ , defined as the ratio between initial mass fraction of fuel on the fuel side,  $Y_{\text{fu},0}$ , and initial mass fraction of oxidizer on the oxidizer side,  $Y_{\text{ox},0}$ , divided by corresponding values for stoichiometric combustion [1]. Values of  $\phi$  varied between 0.5 and 1.6.

The lower nozzle contained a cylindrical tube of constant internal diameter. To vary the size of the generated vortex ring, four different tubes with inner diameters of 0.5, 2, 5, and 10 mm were used. The tube was connected to a cylindrical plenum chamber in which a piston is moved by an actuator. We could vary the volume of fluid pushed by the piston and the piston rise time, which allowed control of the vortex speed. By separately changing the tube size and the actuation parameters, we generated vortex rings with an external radius  $R_{\text{H}}$  that varied from 0.76 mm to 11.2 mm, and with a propagation speed  $U_{\text{T}}$  that varied from 0.22 m/s to 5.05 m/s. Both the vortex size and the vortex speed were measured using the same setup (with pure nitrogen injection in the upper burner) by planar laser-induced fluorescence (PLIF) of acetone, with acetone injected through the vortex generator and all other conditions similar to the standard experiment [21]. It is known that the rotational velocity and the propagation speed of a vortex ring are closely connected in this configuration.

Measurements were carried out mainly using PLIF of the OH radical simultaneously with Rayleigh scattering. The PLIF of OH relied on a frequency-doubled Nd:YAG laser at 532 nm (800 mJ power), which was used to excite OH (281.3 nm absorption line) via a frequency-doubled rhodamine dye laser. The fluorescence signal was filtered using WG 295 and UG 11 filters and was subsequently collected on an intensified charge-coupled device

(CCD) camera with  $576 \times 384$  pixels. For simultaneous Rayleigh measurements, 300 mJ of energy was employed to pump the dye laser used to excite the OH radical. The remaining 500 mJ was separated at the output of the frequency doubler and used for Rayleigh scattering measurements. The Rayleigh signal was collected on a CCD camera ( $512 \times 512$  array) with a bandpass filter centered at 532 nm [22,23].

We also made simultaneous OH PLIF and PIV measurements. The OH PLIF technique was identical to that described previously, with 30 mJ of energy at 532 nm after the frequency-doubled Nd:YAG laser being used to pump the dye laser for the OH PLIF measurements. At the output of a DCM dye laser pumped by a second Nd:YAG system, 40 mJ of energy was produced at 640 nm. The resulting green and red light sheets induced Mie-scattering signals that were collected on a Kodak DCS 460 color CCD camera with  $3060 \times 2036$  pixels. The PIV system relied on a two-color numerical intercorrelation technique. The delay between the two laser shots was equal to 10  $\mu\text{s}$ . All details concerning the simultaneous OH PLIF and PIV measurements have been described elsewhere [21,24].

Experiments were conducted as follows: a steady flame was first established; then, at a selected instant,  $t_0$ , a toroidal vortex was injected impulsively by the action of the piston and accelerated rapidly toward the flame. At a well-defined instant,  $t_1 \geq t_0$ , the signals (either OH PLIF and Rayleigh or OH PLIF and PIV) were collected. Since the experiment was reproducible to within less than 10  $\mu\text{s}$ , the whole temporal interaction sequence was obtained by choosing different delays,  $t_1 - t_0$ .

### Postprocessing of Experimental Results

To increase the signal-to-noise ratio, the pixels of the CCD camera used to collect the OH PLIF signal were paired in two directions, resulting in a real image of  $288 \times 192$  pixels. As explained in Ref. [3] and demonstrated in Ref. [2], it is possible to analyze the PLIF results for the OH radical to compute an instantaneous flame-surface area. This information was used as a complement to a visual examination of the raw results obtained with the CCD camera, allowing us to quantify the wrinkling of the flame front by the vortices and to determine whether extinction was occurring.

Computation of the flame-surface area was automated using MATLAB and has been validated on test pictures. We computed the instantaneous flame-surface area,  $\mathcal{A}(t)$ , in this manner. We removed from  $\mathcal{A}(t)$  the initial value of the flame-surface area for the unperturbed flame,  $\mathcal{A}(0)$ , to obtain  $\mathcal{A}_{\text{n}}(t)$ . To take into account the varying size of the vortex rings, we also considered a normalized flame-surface area,

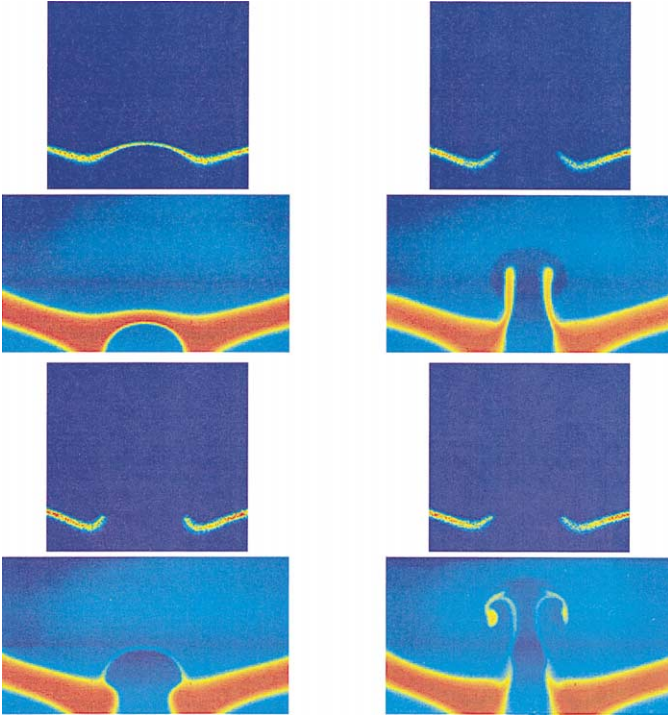


FIG. 1. Simultaneous OH PLIF and Rayleigh measurements. In this case (injector of 5 mm,  $\phi = 0.5$ ), extinction is observed on the symmetry axis. We show at four different interaction times ( $t = 16$  ms, top left;  $t = 18$  ms, bottom left;  $t = 20$  ms, top right;  $t = 22$  ms, bottom right) the OH PLIF image on top and the corresponding Rayleigh diffusion image below it. Note that the colors have been inverted for the Rayleigh signal.

which is more appropriate for examining the influence of small vortices. To accomplish this,  $\mathcal{A}_n(t)$  was divided by a reference surface,  $\mathcal{A}_{\text{ref}}$ , associated with the employed vortex ring. We checked that the structure of our vortex rings was similar to Hill's spherical vortices [25]; therefore, we chose to define  $\mathcal{A}_{\text{ref}}$  as  $2\pi R_H^2$ , with  $R_H$  being the radius of the vortex ring. We then followed in time the evolution of the normalized flame-surface area  $\mathcal{A}^*(t) = (\mathcal{A}(t) - \mathcal{A}(0))/\mathcal{A}_{\text{ref}}$ . Using  $\mathcal{A}^*$ , a small vortex ring may have a large (relative) influence on the flame front, which is not visible with  $\mathcal{A}_n$ . In particular, we have often observed that quite small vortices may increase the flame-surface area by more than 10 times  $\mathcal{A}_{\text{ref}}$ . This confirms that a large number of small vortices may play an important role in the mixing process, showing the importance of taking micromixing into account for non-premixed turbulent flames. Nevertheless, the global impact of a single vortex on the flame is given by the evolution of  $\mathcal{A}_n(t)$ .

Because the inhomogeneities across the laser sheet have not been measured and the cross sections of the different species in the flame differ, our Rayleigh measurements are of a qualitative nature. An example of simultaneous OH PLIF/Rayleigh measurements is shown in Fig. 1. Both diagnostics give complementary pictures of the same interaction process. The OH PLIF signal is associated with the perturbation of the reaction zone, while the Rayleigh signal corresponds to changes in temperature.

The velocity field obtained from PIV measurements was determined by an intercorrelation procedure, with a variable mesh size that depends on the seeding density, the local velocity gradients, and the size of the particle images. To obtain acceptable results, we made sure that the displacement of the particles between the two images was less than half the mesh size. Four or five pairs of particles are then sufficient to obtain accurate results [26]. The intercorrelation peak is found by a search of maximum intensity. Erroneous velocity vectors are then eliminated. This procedure has been described elsewhere [21,24].

Because of the amount of information associated with the PIV measurements, we have to date been unable to postprocess them further. Therefore, we have taken into account in our interpretation only the observed velocity field (Fig. 2). In the near future, we will compute quantities of interest such as instantaneous local strain rate and combine them with an estimation of the curvature to obtain values of the stretch rate exerted on the flame.

### Observed Regimes and Interaction Diagram

Using theoretical results along with the information described above, we have identified eight interaction regimes for the non-premixed flame-vortex interaction (Fig. 3). These regimes reflect the relative importance of the physical phenomena that play

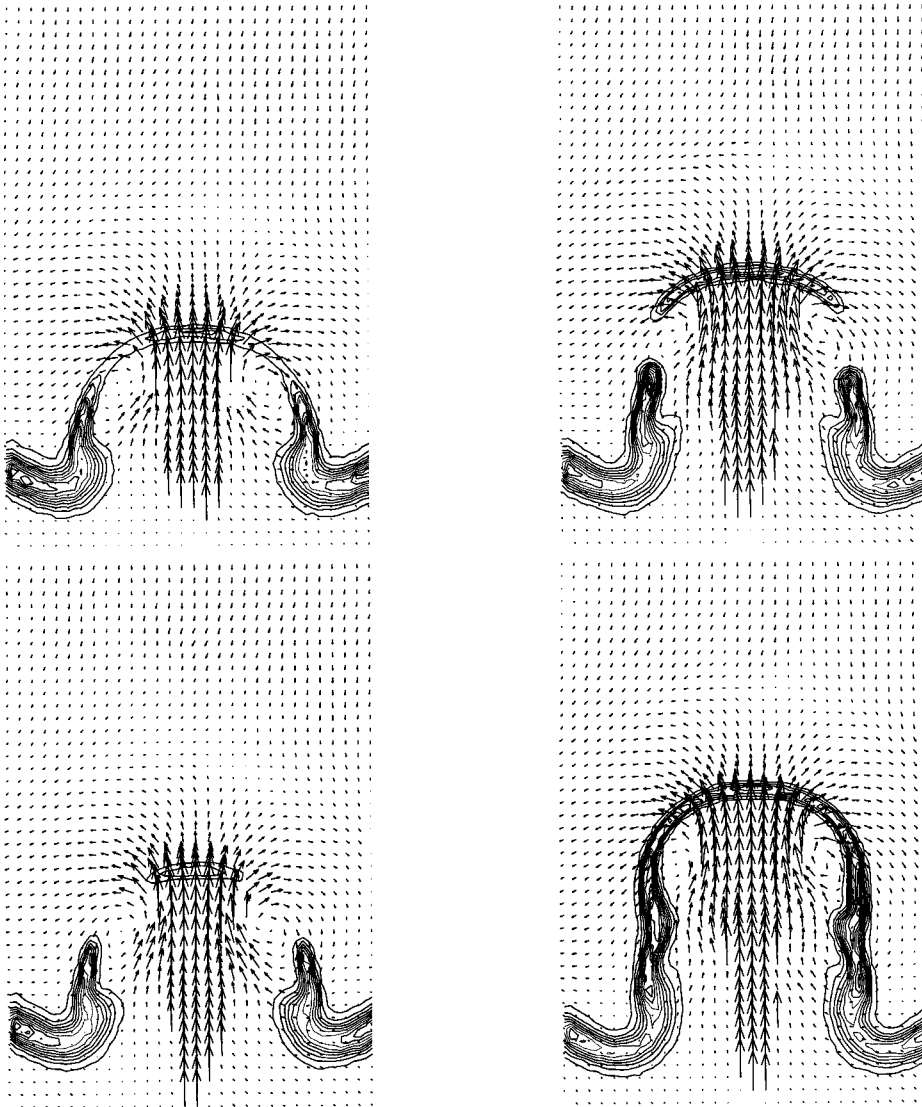


FIG. 2. Simultaneous OH PLIF and PIV measurements. In this case (injector of 5 mm,  $\phi = 1.0$ ), an annular extinction is observed. Shown at four different interaction times ( $t = 8.3$  ms, top left;  $t = 8.5$  ms, bottom left;  $t = 9.0$  ms, top right;  $t = 9.4$  ms, bottom right) are the isolevels of OH obtained by PLIF and the corresponding velocity vectors obtained by PIV. The lowest OH isolevel corresponds to the extinction limit [3].

a major role in this configuration: dissipation, straining, curvature, wrinkling, roll-up, and quenching. We have plotted the results in a spectral diagram, similar to that in Refs. [9,11,27]. To facilitate comparison, we kept the coordinates used in Ref. [27]. The domain accessed using our experimental setup is also displayed in Fig. 3.

The horizontal axis of this diagram corresponds to the ratio of the diameter of the vortex ring  $2R_H$  to

the initial thermal flame width  $\delta_f$ . The vertical axis is associated with the ratio of the characteristic flame time  $t_c$  to the propagation time of the vortex through the flame  $\delta_f/U_T$ . The flame time,  $t_c$ , is not easy to define and cannot be measured in our experimental setup. We have chosen here to use the asymptotic theory results of Ref. [28] to compute this flame time as a function of the global mixture ratio,  $\phi$ . We obtain

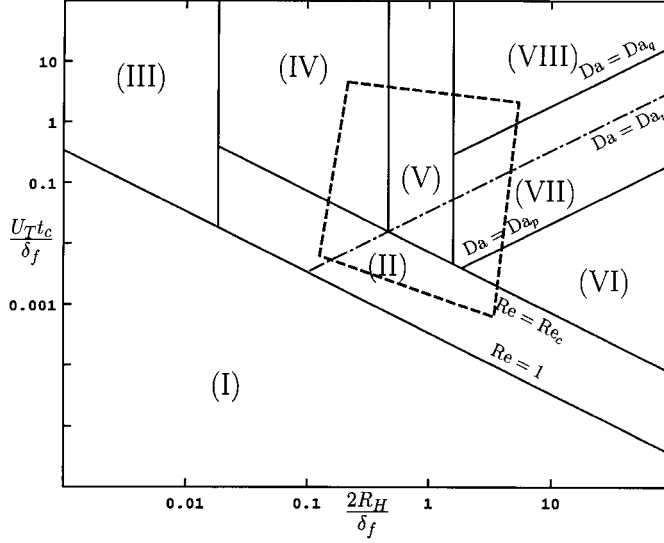


FIG. 3. Spectral diagram for the non-premixed flame-vortex interaction (log-log scale). This diagram is a synthesis of our experimental results along with theoretical considerations. Eight interaction types are identified. In zones I, II, and III, the vortices have no effect or a very weak effect on the flame. In zone IV, moderate curvature and wrinkling effects are observed. In zone V, a thickening of the reaction zones along with strong curvature effects and wrinkling is observed, leading to extinction. Zone VI is associated with wrinkling effects and a strong roll-up of the reaction zones, without extinction. Zone VII is similar to zone VI except that pockets of oxidizer are formed and burn in the fuel part of the domain. Finally, in zone VIII, wrinkling and roll-up are still important, but extinction is observed always on the centerline. The domain limited by the dashed line corresponds to the zone accessible with our experimental setup.

TABLE 1  
Characteristic flame time obtained by asymptotic analysis for a nonpremixed hydrogen/air flame.<sup>1</sup>

$\phi$	0.5	0.6	0.7	0.8	0.9	1.0
$t_c^{-1} (s^{-1})$	$1.42 \cdot 10^2$	$4.30 \cdot 10^2$	$1.21 \cdot 10^3$	$2.11 \cdot 10^3$	$3.84 \cdot 10^3$	$6.29 \cdot 10^3$
$\phi$	1.1	1.2	1.3	1.4	1.5	1.6
$t_c^{-1} (s^{-1})$	$9.58 \cdot 10^3$	$1.40 \cdot 10^4$	$1.97 \cdot 10^4$	$2.63 \cdot 10^4$	$3.37 \cdot 10^4$	$4.27 \cdot 10^4$

<sup>1</sup>The Arrhenius pre-exponential factor has been adapted to obtain the correct extinction limit for  $\phi = 0.7$ .

$$\frac{1}{t_c} = \phi A \left( \frac{\rho_f}{\rho_{ox,0}} \right)^2 Le_F K^2 \left( \frac{C_p T_f^2}{Q Y_{fu,0} T_a} \right)^2 \exp \left( - \frac{T_a}{T_f} \right) \quad (1)$$

where  $T_f$  and  $\rho_f$  correspond to the temperature and density at the flame [28]. The fuel Lewis number,  $Le_F$ , introduced here is taken to be equal to 0.3 [29]. The factor  $K$  is necessary for taking into account the different Lewis numbers of the fuel and oxidizer [28]. Finally, the activation temperature,  $T_a$ , is taken to be 8000 K, and the ratio of specific heat release to heat capacity  $Q/C_p$  is taken to be  $5 \times 10^4$  K [30,31]. The Arrhenius pre-exponential factor,  $\mathcal{A}$ , of the single reaction used to describe the chemical

processes has been chosen to obtain the correct extinction limit for a global mixture ratio  $\phi = 0.7$ . Since these values of  $t_c$  are obtained by high activation energy asymptotics with a single-step irreversible reaction, they yield only an order of magnitude approximation. The computed characteristic flame times using our set of parameters are given in Table 1.

In Fig. 3, we have also plotted some theoretical lines given in Ref. [27], corresponding to different values of the Reynolds number ( $Re$ ) and Damköhler number ( $Da$ ). The line associated with  $Re = (2R_H)U_T/\nu = 1$  is the limit of instantaneous vortex dissipation by viscosity (for  $Re < 1$ ). This line has a slope of  $-1$  in this log-log diagram.

The line  $Da = Da_q$  corresponds to the quenching limit. It can also be defined as

$$\frac{U_T t_c}{\delta_f} = \frac{1}{Da_q} \frac{2R_H}{\delta_f} \quad (2)$$

Extinction is observed for  $Da < Da_q$ .

The line  $Da = Da_n$  corresponds to the limit for unsteady effects. It can also be defined as  $U_T t_c / \delta_f = (1/Da_n)(2R_H/\delta_f)$ . Unsteady effects should be strong for  $Da < Da_n$ .

We have also plotted the vertical line  $(2R_H)/\delta_f = 2$ . It corresponds intuitively to the limit for cases where curvature effects are strong (for  $(2R_H)/\delta_f < 2$ ), since larger vortices will not significantly curve the flame front.

Zone I corresponds to values of the vortex with  $Re < 1$ . It is well known from theoretical considerations that such vortices are dissipated immediately by viscosity [32] and, therefore, do not influence the flame. We did not observe this precise behavior in our experiments. In fact, it appears that this no-effect zone is not associated with  $Re = 1$ , but with a somewhat higher cut-off value of  $Re = Re_c$ . If we choose arbitrarily as a definition of *no-effect* that the maximum increase of flame surface area  $\mathcal{A}_n(t)$  during the interaction is less than  $8\pi R_H^2$ , we obtain  $Re_c = 23$  experimentally for our setup. Zone II corresponds to that part of the domain between  $Re = 1$  and  $Re = Re_c$ .

In zone III, the Reynolds number of the vortices is larger than 1, but these vortices do not survive sufficiently long to perturb the flame before being dissipated by viscosity. This corresponds to a condition

$$\frac{(2R_H)^2}{\nu} < t_c \quad (3)$$

After introducing the Prandtl number ( $Pr$ ) and the  $Da$  that is characteristic of thermal-diffusion effects, that is,  $Da_d = \rho C_p \delta_f^2 / (\lambda t_c)$ , the limit of this zone corresponds to a ratio of vortex size to flame width equal to

$$\frac{2R_H}{\delta_f} = \left( \frac{Pr}{Da_d} \right)^{1/2} \quad (4)$$

This line marks the limit between zone III and zone IV. This limit could not be verified in our experiments because it is impossible to generate sufficiently small vortices. In fact, we have verified that it would still be impossible to reach this limit in our setup by increasing the flame width significantly by changing the diluent or placing the entire experiment in a low-pressure vessel.

In zone IV, we have  $(2R_H)/\delta_f < 2$ . Curvature effects are therefore important. However, extinction is not observed because the vortex ring is not large enough to separate the two sides of the induced wrinkle, since  $(2R_H) < \delta_f/2$ . For the same reason, the increase in flame-surface area is not very large, since the produced flame surface remains in the vicinity of the symmetry axis.

Zone V is limited in the horizontal direction by the vertical lines  $(2R_H)/\delta_f = 1/2$  on the left and  $(2R_H)/\delta_f = 2$  on the right. Therefore, in this zone curvature effects are still important. However, since the dimensions of the vortices are of the same order of magnitude as the flame width, we also observed an important thickening of the reaction zone. At the same time, wrinkling effects are now important. As a consequence of curvature effects and of stronger vortices, extinction was observed in this zone, although the corresponding vortices were still small. PLIF images illustrating the thickening of the reaction zone can be found in Ref. [3].

In zone VI, wrinkling effects become strong in comparison with zone II, and curvature effects do not play an important role since the vortices are much larger than the flame thickness. However, an important roll-up of the flame is observed to participate in the increase in flame surface area. No quenching is observed in this zone. Images illustrating this roll-up can be found in Ref. [3].

Zone VII is separated from zone VI by a slanted line  $Da = Da_p$ . The pinch-off of the flame front behind the vortex is essential for generating a pocket and occurs when the vortex characteristic time is shorter than a chemical time  $t_p$  associated with this phenomenon. This condition can be written in terms of the Damköhler number  $Da_p$ , which compares the characteristic time of pocket formation to the flame time as  $(U_T t_c)/\delta_f > (1/Da_p)(2R_H/\delta_f)$ , which also corresponds to the condition  $Da = Da_p$ . Since  $Da > Da_q$  there, we observe no extinction. The wrinkling effect of the vortices on the flame-surface area is still strong in this zone, as in zone VI. Curvature effects are still negligible, but roll-up is again considerable. In zone VII, this roll-up leads eventually to the formation of pockets of oxidizer inside the upper part of the setup, which is filled with diluted fuel. These pockets are continuously surrounded by an active reaction zone.

The theoretical line  $Da = Da_n$  of Ref. [27] runs through zones II, V, and VII. It is not possible in our setup to identify unsteady effects (*unsteady* meaning here that the flame structure is not in equilibrium with the flow field imposed by the vortex). We are, therefore, unable to verify the validity and the importance of this separation in our experiments.

Finally, zone VIII is separated from zone VII by the slanted line  $Da = Da_q$ . We, therefore, observe extinction due to strain in zone IX, since  $Da < Da_q$ . The results shown in Fig. 1 correspond to this zone, while Fig. 2 is associated with the boundary between zones V, VII, and VIII. The influence of the vortices on the flame-surface area is still strong; roll-up effects are observed again, while curvature effects are negligible. As a result of extinction of the flame induced by strain and although pockets of oxidizer can still be formed in this zone, we did not observe the burning of such pockets in the fuel side of the setup.

These results are summarized in Fig. 3. This spectral diagram can be used to establish a turbulent, non-premixed combustion diagram. To accomplish this, we considered that a non-premixed flame front interacting with a turbulence field was submitted to the effect of a continuous distribution of vortices, the size and velocity of which varied from the Kolmogorov scale to the integral scale. This means that at each point of a turbulent combustion diagram, we must associate information from the spectral diagram, where the influence of all the corresponding turbulent scales was taken into account [11,33]. By doing so, we assumed that each vortex acts independently on the flame front. Possible nonlinear interactions between several vortices were lost in this procedure. Nevertheless, it constituted an interesting step toward a more accurate description of turbulent, non-premixed combustion.

If one considers the classical relations for homogeneous isotropic turbulence [32], the relation between the integral length scale  $l_t$  and the Kolmogorov length scale  $l_k$  is  $l_t = Re_r^{3/4}/l_k$ . Similarly, the integral velocity fluctuation  $u'$  is related to the Kolmogorov velocity  $u_k$  by  $u' = Re_r^{1/4}u_k$ . As a consequence, the energetic cascade for homogeneous, isotropic turbulence is represented by a straight line of slope 1/3 in our spectral diagram. Moreover, the existing line  $Re = 1$  corresponds readily to the Kolmogorov scales, which means that the starting point of the segment representing the turbulent energy distribution will be located on this line. We need only to compute the point on the spectral diagram associated with the integral scales to determine the information needed to place this segment. Depending on the different zones that this segment will cross, it is then possible to deduce the turbulent, non-premixed combustion regime associated with these turbulence parameters. This work and the associated interpretation are presently underway.

### Conclusions

Using various optical diagnostic techniques on a flexible setup, we have investigated in detail the interaction of a vortex ring and a planar, non-premixed, diluted hydrogen/air flame. Data were obtained by varying mainly the global mixture ratio of the flame and the size and propagation speed of the vortex ring. Plotting these results in a single spectral interaction diagram and using theoretical considerations for zones where no experimental points were available, we have identified eight interaction regimes. These regimes correspond to the balance between the physical phenomena that control non-premixed flame-vortex interactions: dissipation, straining, curvature, wrinkling, roll-up, and extinction. This spectral diagram can be employed eventually to build a turbulent, non-premixed combustion diagram.

### Acknowledgments

Travel of researchers between Ecole Centrale and Wright-Patterson has been supported by the Windows-on-Science program. The Ph.D. work of P.-H. Renard has been supported financially by DRET. This work was also supported partly by U.S. Air Force Contract F33615-95-C-2507. The authors thank Drs. Cam Carter (ISSI) and Jeff Donbar (AFRL) for their advice and assistance with PLIF, PIV, and Rayleigh-scattering measurements [34].

### REFERENCES

1. Thévenin, D., Rolon, J. C., Renard, P. H., Kendrick, D. W., Veynante, D., and Candel, S., *Proc. Combust. Inst.* 26:1079–1086 (1996).
2. Thévenin, D., Renard, P. H., Rolon, J. C., and Candel, S., *Proc. Combust. Inst.* 27:719–726 (1998).
3. Renard, P. H., Rolon, J. C., Thévenin, D., and Candel, S., *Combust. Flame* 117:189–205 (1999).
4. Renard, P. H., Thévenin, D., Rolon, J. C., and Candel, S., *Prog. Energy Combust. Sci.* 26:225–282 (2000).
5. Karagozian, A. R., and Manda, B. V. S., *Combust. Sci. Technol.* 49:185–200 (1986).
6. Jarosinski, J., Lee, J. H. S., and Knystautas, R., *Proc. Combust. Inst.* 22:505–514 (1988).
7. Roberts, W. L., and Driscoll, J. F., *Combust. Flame* 87:245–256 (1991).
8. Rutland, C. J., and Ferziger, J. H., *Combust. Flame* 84:343–360 (1991).
9. Roberts, W. L., Driscoll, J. F., Drake, M. C., and Goss, L. P., *Combust. Flame* 94:58–69 (1993).
10. Katta, V. R., Carter, C. D., Fiechtner, G. J., Roquemore, W. M., Gord, J. R., and Rolon, J. C., *Proc. Combust. Inst.* 27:587–594 (1998).
11. Poinot, T., Veynante, D., and Candel, S., *J. Fluid Mech.* 228:561–606 (1991).
12. Renard, P. H., Rolon, J. C., Thévenin, D., and Candel, S., *Proc. Combust. Inst.* 27:659–666 (1998).
13. Karagozian, A. R., Sugauma, Y., and Strom, B. D., *Phys. Fluids* 31:1862–1871 (1988).
14. Strawa, A., and Cantwell, B., *Phys. Fluids* 28:2317–2320 (1985).
15. Gutmark, E., Parr, T. P., Parr, D. M., and Schadow, K. C., "Vortex Dynamics in Diffusion Flames," paper 7–3, Sixth Symposium on Turbulent Shear Flows, Toulouse, France, 1987.
16. Chen, L. D., Roquemore, W., Goss, L. P., and Vilimpoc, V., *Combust. Sci. Technol.* 77:41–57 (1991).
17. Hsu, K. Y., Chen, L. D., Katta, V. R., Goss, L. P., and Roquemore, W. M., "Experimental and Numerical Investigations of the Vortex-Flame Interactions in a Driven Jet Diffusion Flame," AIAA paper 93-0455, Thirty-First Aerospace Sciences Meeting, January 11–14, 1993.
18. Park, J., and Shin, H. D., *Combust. Flame* 110:67–77 (1997).

19. Chen, S., and Dahm, W., *Proc. Combust. Inst.* 27:2579–2586 (1998).
20. Rolon, J. C., Aguerre, F., and Candel, S., *Combust. Flame* 100:422–429 (1995).
21. Fiechtner, G. J., Renard, P. H., Carter, C. D., Gord, J. R., and Rolon, J. C., *J. Visualization* 2:331–342 (1999).
22. Gord, J. R., Donbar, J. M., Fiechtner, G. J., Carter, C. D., Katta, V. R., and Rolon, J. C., “Experimental and Computational Visualization of Vortex-Flame Interactions in an Opposed-Jet Burner,” paper AB-082, International Conference on Optical Technology and Image Processing in Fluid, Thermal and Combustion Flow, Visualization Society of Japan and SPIE, Yokohama, Japan, 1998.
23. Gord, J. R., Donbar, J. M., Fiechtner, G. J., Carter, C. D., and Rolon, J. C., in *Ninth International Symposium on Applications of Laser Techniques to Fluid Mechanics*, Lisbon, Portugal, 1998, pp. 35.1.1–35.1.8.
24. Fiechtner, G. J., Carter, C. D., Grinstead, J., Gord, J. R., Roquemore, W. M., and Rolon, J. C., “Flame-Vortex Interactions in a Non-Premixed H<sub>2</sub>/N<sub>2</sub>/Air Counterflow Burner,” AIAA paper 98-3770, AIAA/ASME/SAE/ASEE Thirty-Fourth Joint Propulsion Conference, 1998.
25. Saffman, P., *Vortex Dynamics*, Cambridge University Press, Cambridge, U.K., 1992.
26. Gogineni, S., Goss, L., Pestian, D., and Rivir, R., *Exp. Fluids* 25:320–328 (1998).
27. Cuénot, B., and Poinso, T., *Proc. Combust. Inst.* 25:1383–1390 (1994).
28. Cuénot, B., and Poinso, T., *Combust. Flame* 104:111–137 (1996).
29. Zhao, J., Isaac, K., and Pellett, G., *J. Propul. Power* 12:534–542 (1996).
30. Coffee, T. P., Kotlar, A. J., and Miller, M. S., *Combust. Flame* 54:155 (1983).
31. Thévenin, D., and Candel, S. M., *Phys. Fluids A* 7:434–445 (1995).
32. Hinze, J. O., *Turbulence, 2nd Ed.*, McGraw-Hill, New York, 1975.
33. Poinso, T., Veynante, D., and Candel, S., *Proc. Combust. Inst.* 23:613–619 (1990).
34. Carter, C. D., Donbar, J. M., and Driscoll, J. F., *Appl. Phys. B* 66:129–132 (1998).

## COMMENTS

*William Roberts, North Carolina State University, USA.* In the region where you see strong extinction from large, strong vortices, is there any evidence of a triple-flame structure on the leading edges as the flame recovers?

*Author's Reply.* We never observed triple flames in our experiments; we only have information regarding the temperature, velocity, and OH concentration. Such data are

not sufficient to detect the possible presence of triple flames. In our direct numerical simulations using detailed chemistry and transport models, multibrachial flames do appear on the edges of the extinction hole but are clearly visible only on the profiles of the HO<sub>2</sub> and H<sub>2</sub>O<sub>2</sub> radicals.